PAPER

Soft X-ray characterization of $Zn_{1-x}Sn_xO_y$ electronic structure for thin film photovoltaics

Mukes Kapilashrami,[a] Coleman X. Kronawitter,[bc] Tobias Törndahl,[d] Johan Lindahl,[d] Adam Hultqvist,[d] Wei-Cheng Wang,[ae] Ching-Lin Chang,[e] Samuel S. Mao[bc] and Jinghua Guo*[a]

Zinc tin oxide ($Zn_{1-x}Sn_xO_y$) has been proposed as an alternative buffer layer material to the toxic, and light narrow-bandgap CdS layer in $CuIn_{1-x},Ga_xSe_2$ thin film solar cell modules. In this present study, synchrotron-based soft X-ray absorption and emission spectroscopies have been employed to probe the densities of states of intrinsic ZnO, $Zn_{1-x}Sn_xO_y$ and SnO_x thin films grown by atomic layer deposition. A distinct variation in the bandgap is observed with increasing Sn concentration, which has been confirmed independently by combined ellipsometry-reflectometry measurements. These data correlate directly to the open circuit potentials of corresponding solar cells, indicating that the buffer layer composition is associated with a modification of the band discontinuity at the CIGS interface. Resonantly excited emission spectra, which express the admixture of unoccupied O $2p$ with Zn $3d$, $4s$, and $4p$ states, reveal a strong suppression in the hybridization between the O $2p$ conduction band and the Zn $3d$ valence band with increasing Sn concentration.

Introduction

Among all solar energy conversion technologies, thin film photovoltaic (PV) devices have attracted persistent attention because they provide a direct pathway for generation of electrical energy from solar energy with high efficiency and low material cost. The highest efficiency for this class of PV devices is found for those based on the absorbing chalcopyrite compound $CuIn_{1-x}Ga_xSe_2$ (CIGS), whose reported efficiency values reach 20%.[1,2] In contrast to p–n junction Si-based PV, thin film devices possess relatively complex architectures, wherein heterojunctions, and associated interfacial band discontinuities, are responsible for carrier separation. The design and optimization of layers in such devices, where successful integration of new materials requires careful consideration of compatibility with the entire structure, is best facilitated by direct evaluation of the density of states of the constituent materials. This is especially true for design of the so-called buffer layer, commonly a CdS layer inserted between the absorbing

chalcopyrite phase and the transparent conductive electrode. The CdS-CIGS interfacial region has been shown, using elementally-resolved X-ray spectroscopies, to possess a graded composition and complex electronic structure, which is known to be crucial to the efficient operation of the device.[3]

Inclusion of the CdS layer is unfavorable for mass production of CIGS-based devices because of its prohibitive toxicity, the involvement of a non-vacuum chemical bath deposition (CBD) step, and its absorption of blue light, related to its moderately small bandgap of 2.4–2.5 eV. Extensive research is conducted to develop suitable replacements for CBD-CdS. ZnO-based compounds (*e.g.* $ZnO_{1-x}S_x$, $Zn_{1-x}Mg_xO$ and $Zn_{1-x}Sn_xO_y$) and In_2S_3 show efficiencies comparable to those of reference devices using CdS.[4–6] $Zn_{1-x}Sn_xO_y$ is a new promising amorphous buffer layer for CIGS solar cells developed at the Ångström Solar Center (ÅSC) Uppsala University, Sweden.[6,7]

ZnO is well-known for its optical and electronic properties, which include a wide (direct) bandgap (E_g) near the UV range (*ca.* 3.37 eV), a high exciton binding energy at room-temperature (*ca.* 60 meV, almost twice that of GaN), and a high solubility of dopant atoms (up to *ca.* 30%, depending on the method of preparation).[8–11] Even though the implemented ZnO-based buffer layers absorb fewer incoming photons, due to their larger optical bandgaps compared to that for CdS, the reported solar cell efficiency values are still not markedly higher than those containing CdS.[4] This observation suggests that additional in-depth studies of the atomic and electronic

[a] *Advanced Light Source, Lawrence Berkeley National Laboratory, Berkeley, CA 94720, USA. E-mail: jguo@lbl.gov*
[b] *Department of Mechanical Engineering, University of California at Berkeley, Berkeley, CA 94720, USA*
[c] *Environmental Energy Technologies Division, Lawrence Berkeley National Laboratory, Berkeley, CA 94720, USA*
[d] *Ångström Solar Center, Uppsala University, Box 534, SE-751 21 Uppsala, Sweden*
[e] *Department of Physics, Tamkang University, Tamsui, Taiwan 25137, Republic of China*

10154 | *Phys. Chem. Chem. Phys.*, 2012, **14**, 10154–10159

This journal is © the Owner Societies 2012

structures of the ZnO-based buffer layers are important in order to understand and improve the performance of the solar cell device. We present herein a systematic experimental study of the electronic and optical properties of $Zn_{1-x}Sn_xO_y$ thin films ($0 \leq x < 0.31$), deposited on Si (001) substrates by atomic layer deposition (at ÅSC), using synchrotron-based soft X-ray spectroscopies on Beamline 7.0.1 at the Advanced Light Source, Lawrence Berkeley National Laboratory.

X-ray spectroscopy is a powerful tool in which the interaction of light (photons) and matter is used to probe the electronic structure of materials (both bulk and at reduced scale). Tuning the wavelength of incident light (*i.e.* the photon energy) enables the element-selective study of solid materials as the energy separations at core levels differ from element to element.[12] Two such spectroscopic techniques are X-ray absorption spectroscopy (XAS) and X-ray emission spectroscopy (XES). XAS is a technique used to characterize matter by evaluation of unoccupied electronic states as a result of excitation of core electrons into higher unoccupied states (conduction band), or into the free unbound state. Whereas XES probes the occupied states (valence band) by monitoring the emission (as core holes are populated by electrons from the valence orbital) probability as a function of photon-out. Technological advances have made it possible to produce high-brilliance light ranging from ultraviolet, soft X-ray, to hard X-ray, making it possible to study a broader selection of elements and compounds in more detail.[12] In this present study, O $1s$ XAS spectra have been obtained by measuring the photocurrent (total electron yield, TEY) directly on the sample (with a resolution of 0.2 eV) across the excitation energy range of 500–590 eV. XES spectra have been acquired using a high-resolution grazing-incidence grating spectrometer at an excitation energy of 585 eV.[13]

Experiment

A microchemistry F-120 ALD (atomic layer deposition) reactor operated at a deposition temperature of 120 °C has been used to grow $Zn_{1-x}Sn_xO_y$ films on silicon substrates. In this study the zinc precursor is diethyl zinc (DEZ, $Zn(C_2H_5)_2$), the tin precursor is TDMASn ($Sn(N(CH_3)_2)_4$) and the oxygen precursor is deionized water (H_2O, 18 MΩ cm). Nitrogen gas, N_2 (99.9999%), is used as the carrier gas for the ALD process. Both water and DEZ effuse into the chamber at room temperature, whereas the Sn precursor requires heating in a water bath to 40 °C to achieve a suitable vapor pressure by sublimation. The ALD process uses a Sn- or Zn-precursor : N_2 : H_2O : N_2 pulse cycle with pulse lengths of 1200 (for Sn and Zn) : 1600 : 400 : 1600 ms, respectively. To control the [Sn]/([Sn] + [Zn]) content of the film the Sn/(Sn + Zn) pulse ratio in the ALD cycle is changed. As an example, a $Zn_{1-x}Sn_xO_y$ 3 : 2 buffer layer uses an average of three DEZ : N_2 : H_2O : N_2 cycles for every two TDMASn : N_2 : H_2O : N_2 cycles and has a Sn/(Sn + Zn) pulse ratio of 0.4.

The thickness of the $Zn_{1-x}Sn_xO_y$ thin films has been determined accurately using a Dual Beam combined scanning electron microscope (SEM)/focused ion beam (FIB) Nova 600 Nanolab (FEI Electron Optics, Acht, Netherlands). The crystal structure and the elemental mapping of the films have been

Table 1 Summary on the ALD process, film composition and surface roughness for the six samples in the present study

Sample ID	ALD pulse ratio Sn/(Sn + Zn)	ALD cycles	EDX composition $Zn_{1-x}Sn_xO_y$ x	Surface roughness (nm)
S1	0	750	0	4.3
S2	0.25	4000	0.13	4.4
S3	0.40	4000	0.18	4.5
S4	0.40	2000	0.20	7.2
S5	0.67	4000	0.31	3.8
S6	1	1400	1	—

characterized respectively by X-ray diffraction (XRD, Bruker D8 Discover; $^{Cu}\lambda_{K\alpha}$: 1.5406 Å) and energy dispersive X-ray spectroscopy (EDXS OXFORD D7021, attached to a high resolution Hitachi 3000N SEM). Surface roughness analysis of the thin films has been performed using an atomic force microscope in AC mode (JSPM 5400, JEOL). See Table 1 for an overview of the samples in this present investigation.

Results and discussion

Structural and elemental characterization

From the XRD characterization it is confirmed that $Zn_{1-x}Sn_xO_y$ thin films are amorphous for doped thin films ($x > 0$), while the intrinsic ($x = 0$) ZnO thin film has a crystalline (with orientation disorder) structure (see Fig. 1a). The inset in Fig. 1a shows the corresponding XRD pattern for the $Zn_{0.87}Sn_{0.13}O_y$ thin film. Fig. 1b shows a typical cross-section image for the $Zn_{0.87}Sn_{0.13}O_y$ thin film acquired by the Dual-Beam FIB system. The average film thickness is measured to be *ca.* 270 nm. All the thin films considered were found to be uniform, with no obvious pinholes, as judged from the cross-section analyses. In this investigation we found the thin films to accumulate charging effects in the presence of the ion/electron beam, indicating that they are highly insulating, which is consistent with previous findings.[6]

Soft X-ray characterization

Fig. 2a displays the O K-edge XAS spectra for the $Zn_{1-x}Sn_xO_y$ thin films, reflecting, through the dipole selection rule, the O $2p$ unoccupied states. No absorption feature is observed prior to A, the features in the region from 530–539 eV (A, B) are mainly attributed to the hybridization between the O $2p$ and Zn $4s$ states, while those at the higher energy interval 539–545 eV
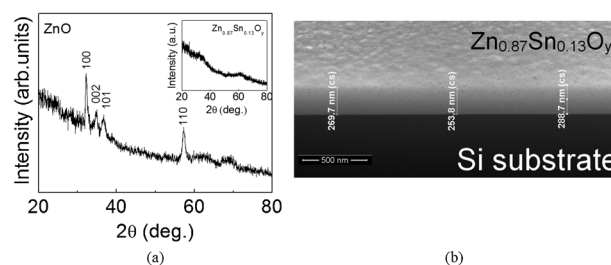

Fig. 1 (a) Typical XRD pattern for the intrinsic ZnO thin film. Inset shows the corresponding pattern for the $Zn_{0.87}Sn_{0.13}O_y$ thin film. (b) Typical cross-section images for the $Zn_{0.87}Sn_{0.13}O_y$ thin film (*ca.* 270 nm).

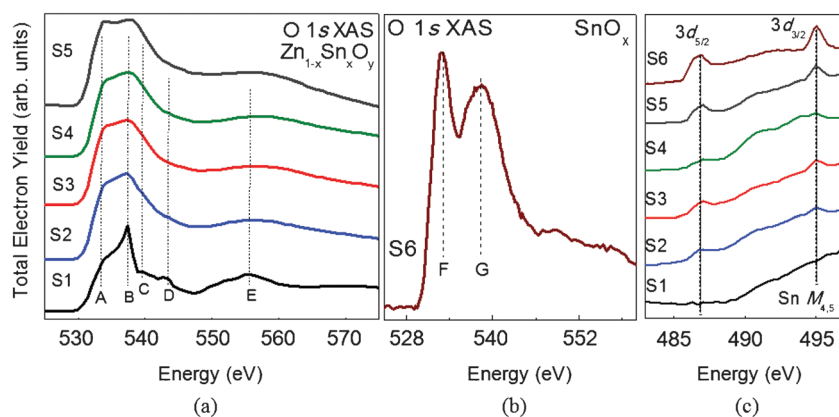**Fig. 2** (a) O *K*-edge absorption spectra for (a) $Zn_{1-x}Sn_xO_y$ and (b) SnO_x thin films. (c) Sn $M_{4,5}$-edge absorption spectra for $Zn_{1-x}Sn_xO_y$.

(C, D) are mainly attributed to O 2p states hybridized with Zn 4p states. At energies greater than 545 eV the contribution is believed to arise from O 2p–Zn 4d states.[13] It is evident in Fig. 2 that the absorption features labeled B–E become less resolved with increasing Sn concentration (*i.e.* a spectral broadening is observed with respect to the intrinsic ZnO) indicating suppression of the hybridization between O 2p states with various energy states of Zn at its substitution of Sn. Such observed spectral broadening of the spectral features has previously been attributed to the presence of oxygen vacancies, where an oxygen vacancy is believed to affect the surrounding shell of the oxygen atoms by effectively altering their 1s binding energies in those subsequent shells surrounding the vacancy site.[14] In addition to the oxygen related defects, the impact of the higher exciton binding energy of SnO_2 (130 meV[15]), which is more than twice that of ZnO, may be considered.

Corresponding O 1s XAS for the SnO_x is shown in Fig. 2b. The most prominent feature at *ca.* 533 eV (F) arises from the O 1s core excitations into the a_g band, thus forming the bottom of the conduction band. The feature at *ca.* 538 eV (G) reflects the hybridization between the O 2p and Sn 5sp states.[16,17] Fig. 2c shows the variation in the Sn $M_{4,5}$-edge absorption spectra as a function of increasing Sn concentration, *i.e.* ZnO → SnO_x, reflecting the electron transitions from the Sn 3d (spin–orbit split into 3$d_{3/2}$ and 3$d_{5/2}$ levels giving rise to the $M_{4,5}$-edge)

core levels into unoccupied electronic states above the Fermi level.[18] Interestingly, the two features reflecting Sn $M_{4,5}$-edge are not as resolved in $Zn_{0.8}Sn_{0.2}O_y$ thin film as in the other $Zn_{1-x}Sn_xO_y$ thin film samples. Such a discrepancy has not been fully understood. However, the combination of its higher surface roughness (*ca.* 7 nm), and smaller film thickness may plausibly contribute to such discrepancy in the electronic structure.

The bandgap of the $Zn_{1-x}Sn_xO_y$ thin films has been extracted by combining their respective XAS and XES spectra. The valence band maxima and the conduction band minima are calculated by extending the linear sections of the respective band to where they intersect with the background.[13] Typical oxygen XES–XAS spectra reflecting densities of states in the valence and conduction band of the ZnO, and $Zn_{0.8}Sn_{0.13}O_y$ thin films are displayed in Fig. 3. The strong features at *ca.* 520–526 eV (admixture of unoccupied O 2p with Zn 3d4p states) in Fig. 3 suggest additional analysis is required to provide a more comprehensive account of the electronic structure of $Zn_{1-x}Sn_xO_y$ thin films. Table 2 summarizes the calculated bandgap in the $Zn_{1-x}Sn_xO_y$ in this present study.

Band alignment of $Zn_{1-x}Sn_xO_y$ relative to ZnO

As evident from this present study (as summarized in Table 2) we find the bandgap to vary significantly as a function

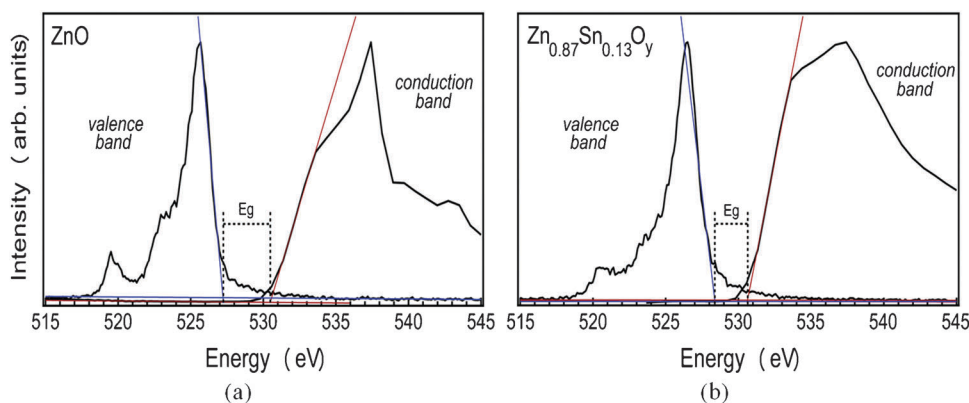**Fig. 3** Typical soft X-ray emission and absorption spectra for (a) intrinsic ZnO, and (b) $ZnO_{0.87}Sn_{0.13}O_y$ thin films probing the valence- and conduction band near the Fermi level.

10156 | *Phys. Chem. Chem. Phys.*, 2012, **14**, 10154–10159

This journal is © the Owner Societies 2012

Table 2 Variation in E_g, ΔE_v ZnO and ΔE_c ZnO as measured by soft X-ray absorption and emission spectroscopy. Corresponding V_{oc} values for $Zn_{1-x}Sn_xO_y$ buffer layers deposited by ALD 2000 cycles in the thickness range 70–100 nm with similar Sn concentrations to ref. 6 are shown as a comparison between the ΔE_c ZnO soft X-ray data and solar cell performance.

Sample	$Zn_{1-x}Sn_xO$ x	E_g (eV)	ΔE_v ZnO (eV)	ΔE_c ZnO (eV)	V_{oc}[5] (V)
S1	0	3.3	0	0	0.383
S2	0.13	2.2	1.2	0.1	0.622
S3	0.18	3.0	0.4	0.2	0.639
S4	0.20	3.0	0.5	0.3	0.647
S5	0.31	2.5	0.8	0.1	0.620
S6	1	2.2	1.0	−0.1	0.316

of Sn concentration, from 3.3 eV for ZnO to 2.2 eV for $Zn_{0.87}Sn_{0.13}O_y$ and SnO_x.

If we consider the ZnO thin film as our reference point (0,0), and study the change in both the valence and conduction band edges as a function of increasing Sn concentration, we find the shift in the valence band edge (ΔE_v) towards higher energies (0 → 1.2 eV) to be the main cause for the reduction in the bandgap in the thin film samples with increasing Sn concentration (see Table 2). A moderate shift in the conduction band edge (ΔE_c) towards higher energies also occurs in all samples (except S6), where a largest ΔE_c value of 0.3 is observed for S4 ($Zn_{0.8}Sn_{0.2}O_y$). The band alignment of the conduction band (ΔE_c), also called conduction band offset (CBO), at the CIGS/buffer layer heterojunction is a critical design aspect of CIGS solar cells. If the CBO is negative (CBO < −0.15 eV), which results in a "cliff", the inversion at the top of the CIGS and the barrier for interface recombination will be reduced, which increases the buffer layer/CIGS interface recombination and thereby lowers the open circuit voltage, V_{oc}, of the device.[19] On the other hand, a large positive CBO (>0.3 eV), which gives rise to a "spike", can lead to lower efficiency due to blocking of the photo current generated in the CIGS.[20] Therefore, the most favorable conduction band alignment, ΔE_c, is found to be slightly positive or close to zero. As shown in Table 2, the ΔE_c relative to ZnO increases with the Sn content in the region 0 < x < 0.2 up to 0.3 eV and decreases again for x = 0.31.

From these data a direct determination of the band alignment between CIGS and $Zn_{1-x}Sn_xO_y$ is not possible given their thickness and deposition on Si substrates. However, the CBO of ALD ZnO deposited on non-graded CIGS with a Ga/(In + Ga) ratio of approximately 0.3 has been determined to be −0.2 eV,[21] whereas the junction ZnO/CdS shows a CBO of −0.3 eV for ZnO in relation to CdS.[22] By using these literature data, the CBO of CIGS/$Zn_{1-x}Sn_xO_y$ is estimated to be slightly positive by 0.1 eV for x = 0.20 and similar to that of CIGS/CdS. A schematic picture of the band alignment between ZnO, $Zn_{1-x}Sn_xO_y$, SnO_x and the literature data of CIGS/ALD-ZnO is shown in Fig. 4. The experimental open circuit voltage (V_{oc}) values from $Zn_{1-x}Sn_xO_y$ solar cells of comparable film composition (as measured by Rutherford back scattering technique) are shown in Table 2. The trend in V_{oc} supports the soft X-ray data by showing an increase in V_{oc} (and solar cell efficiency) as a function of increasing ΔE_c as Sn is added to ZnO up until an x-value of 0.20, where after
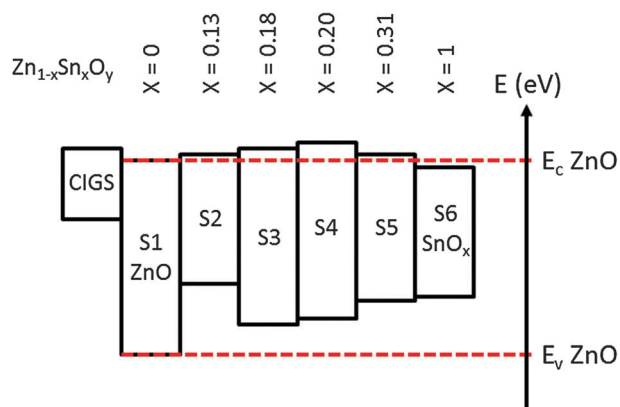

Fig. 4 Band alignment diagram for CIGS/$Zn_{1-x}Sn_xO_y$ heterojunction.

both the ΔE_c and V_{oc} decreases for the sample with x = 0.31. The V_{oc} for the SnO_x sample is similar to that of ZnO. It should also be noted that CBO values change with the surface Ga-content in CIGS, which makes a direct comparison between studies with different CIGS compositions difficult.

Resonant inelastic X-ray spectroscopy

Resonant inelastic X-ray spectroscopy (RIXS) is another emission spectroscopy technique in which the core electrons are resonantly excited to the absorption threshold, and further enables an accurate study of the admixture of unoccupied O 2p states with Zn 3d, 4s, and 4p states.[13] RIXS is distinct in that the final emission is highly dependent on the incident photon energy and carries information on the partial density of occupied states (whereas XES contains information on the density of occupied states).[12] Fig. 5 shows a comparison of the emission O K_α spectra in which the 1s core electrons in the $Zn_{1-x}Sn_xO_y$ thin film samples have been excited at an energy corresponding to their respective absorption edge (as extracted from the absorption spectra in Fig. 2a). Three distinct features are observed in Fig. 5, labeled H–J. The single-band feature H is believed to arise from the mixed states O 2p and Zn 3d, while I and J arises from the mixed states O 2p and Zn 4s and O 2p and Zn 4p respectively.[13] The intensity distribution is more prominent in peaks H and I, and a sequential decrease in the same is observed with increasing Sn concentration. This suggests that a stronger p–d and p–s hybridization exists in the intrinsic ZnO thin film (S1) compared to the $Zn_{1-x}Sn_xO_y$ systems (S2–S5). Keeping the intrinsic ZnO films (S1) as the reference,
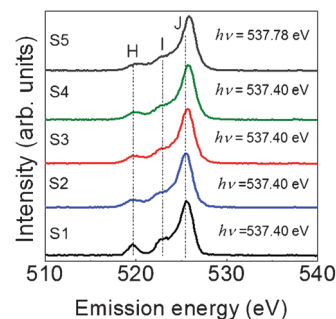

Fig. 5 Variation in the resonantly excited soft X-ray emission spectra with increasing Sn concentration in the $Zn_{1-x}Sn_xO_y$ thin films.

This journal is © the Owner Societies 2012

Phys. Chem. Chem. Phys., 2012, **14**, 10154–10159 | 10157

we find the most intense feature J to shift by *ca.* 0.24 eV in spectrum S5. Only a moderate shift in the same is observed in the other thin films. Such a shift has previously been attributed to the inequivalent positioning of oxygen atoms.[13]

Optical characterization

Optical measurements were performed in atmospheric conditions on a combined ellipsometer-reflectometer (Scientific Computing International Filmtek Par3000SE). The system has a rotating compensator design, which permits measurements with high signal-to-noise ratios, and simultaneously measures the ellipsometric parameters psi (Ψ) and delta (Δ) as well as absolute values for $0°$ (normal incidence) reflectance and $70°$ (oblique angle incidence) reflectance, which are collected by measuring with respect to a reflectance spectrum of a known reference sample (Si). Ellipsometric and $70°$ reflectance data were collected from 330 nm to 1050 nm; $0°$ reflectance data were collected from 240 nm to 1050 nm.

The system's multi-layer film analysis software allows simulation of a multi-layer structure's optical response over the entire spectral range of interest, using a regression analysis to minimize an error function associated with its fit to the measured responses. The multilayer structure employed to simulate the response consisted of a Si substrate and SiO_2 surface layer, whose refractive indices were taken from literature values, followed by the ZnO thin film and its surface layer. The surface layer was modeled with the Bruggeman effective medium approximation (EMA) and consisted of 50% ZnO and 50% void. The software couples the features of the effective medium layer to a computation of surface roughness scattering effects, which are then included in the reflectance simulations. The ZnO films were analyzed by a proprietary model from Scientific Computing International (SCI model[23]), which has previously been used to model the ellipsometric response of ZnO thin films.[24]

The SCI parameterization is similar in a general sense to the Tauc–Lorentz parameterization,[25] which is established in the literature as a method to model the dielectric functions of amorphous materials and semiconductors possessing a band edge transition. However, it differs in a few significant aspects from the Tauc–Lorentz equations. In the Tauc–Lorentz parameterization, the band edge is approximated by the Tauc joint density of states; at energies lower than a constant energy value E_g, the imaginary part of the dielectric function ε_2 is forced to zero. Rather than the constant energy value, the SCI model instead uses a damping term that is itself a function of energy to define the spectral range beyond which optical absorption is absent. Consequently, the band edge dispersion is approximated by a higher order polynomial, which has potential to more realistically represent the band edges of real systems.

The bandgap is quantified by calculating the absorption coefficient α_λ from the imaginary part of the refractive index, followed by an extrapolation of the $(\alpha_\lambda \times \text{thickness})^n$ curve (where $n = 0.5$ for amorphous films and $n = 2$ for direct-gap crystalline films) to the photon energy at which the quantity is equal to zero. Fig. 6 provides the bandgaps calculated in this manner as well as those provided in Table 2 from analyses of the XES-XAS data. The difference in the bandgap predicted
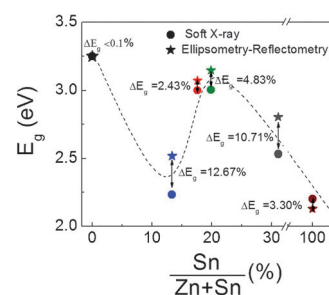

Fig. 6 E_g predicted by ellipsometry-reflectometry (colored stars) plotted with those determined by analyses of soft X-ray spectroscopies (colored circles).

by ellipsometry-reflectometry relative to that predicted by soft X-ray spectroscopy is provided in Fig. 6.

The discrepancies in these predictions involve the differing methodologies between the techniques by which the gap is determined. The bandgap predicted by soft X-ray spectroscopies is based on experimental measurement of relaxations from core-level excitations, and as such provides an accurate physical representation of the materials' occupied and unoccupied electronic structures. The energy distances between features in XES and XAS data are equal to corresponding distances in the actual system density of states.[26]

Bandgaps obtained by combined ellipsometry-reflectometry are quantified by mathematical analyses of the simulated imaginary parts of the refractive indices. Good agreement with the bandgaps predicted by soft X-ray spectroscopies is obtained, especially for crystalline zinc oxide. The quantified energy gaps in amorphous samples were consistently over-estimated using ellipsometry-reflectometry (with the exception of SnO_x). This is most likely an indication that the simulation process ignores certain weak contributions to the densities of states near the band edges, which are not evident in the optical responses; such features are therefore not represented mathematically by the dispersion relations implemented.

Conclusion

In summary, the optical and structural properties of $Zn_{1-x}Sn_xO$ thin films deposited by atomic layer deposition have been investigated. It is found that the intrinsic ZnO possesses a crystalline structure, whereas the SnO_x and $Zn_{1-x}Sn_xO_y$ films are amorphous. Analysis of O K-edge XAS spectra indicates that the formation of oxygen-related defects increases with increasing Sn concentration in the thin films. Similarly, a shift in the O $2p$–Zn $4p$ hybridized states towards higher energies with increasing Sn content is observed in the RIXS spectra, which is believed to arise from inequivalent chemical sites of oxygen atoms. Such inequivalent positioning may be attributed to both oxygen vacancies as well as the amorphous structure of the $Zn_{1-x}Sn_xO_y$ thin films. Strong O $2p$–Zn $3d$ hybridization in the intrinsic ZnO films is evident from the corresponding RIXS spectrum, and is found to decrease as the Zn is substituted by Sn. We find the bandgap (by means of soft X-ray spectroscopy analysis) to vary from 3.3 eV (ZnO) → 2.5 eV ($Zn_{0.87}Sn_{0.13}O_y$) → 2.2 eV (SnO_x), which is in good agreement to those obtained by combined

ellipsometry-reflectometry. This change in the bandgap is found to mainly result from a shift in the valence band edge towards higher energies with increasing Sn concentration, whereas only a moderate shift is observed in the conduction band edge with the same. The shift in the conduction band edge has been found to increase by 0.3 eV for a $Zn_{0.80}Sn_{0.20}O_y$ sample as compared to ZnO, where after it decreased to 0.1 eV for a thin film with a higher Sn content ($Zn_{0.69}Sn_{0.31}O_y$). By comparing to literature data for experimental band alignment determinations of CIGS/ALD-ZnO and CdS/ZnO, a maximum ΔE_c value of 0.1 eV is estimated at the CIGS/$Zn_{0.80}Sn_{0.20}O_y$ interface. The obtained ΔE_c values were also found to correlate well to the open circuit voltage (V_{oc}) values of $Zn_{1-x}Sn_xO_y$-based solar cells, where the V_{oc} of the solar cell devices increased with increasing ΔE_c. An in-depth study of the interface $Zn_{1-x}Sn_xO_y$/CIGS will provide additional information on the occurrence of any intermixing at the interface, which may affect the band overlap, thus shed additional light on the current intriguing task of tailoring the band structure of ZnO-based compounds with respect to the CIGS absorber layer.

Acknowledgements

References

1 P. Jackson, D. Hariskos, E. Lotter, S. Paetel, R. Wuerz, R. Menner, W. Wischmann and M. Powalla, *Prog. Photovoltaics*, 2011, **19**, 894.

2 I. Repins, M. A. Contreras, B. Egaas, C. DeHart, J. Scharf, C. L. Perkins, B. To and R. Noufi, *Prog. Photovoltaics*, 2008, **16**, 235.

3 S. Pookpanratana, I. Repins, M. Bär, L. Weinhardt, Y. Zhang, R. Félix, M. Blum, W. Yang and C. Heske, *Appl. Phys. Lett.*, 2010, **97**, 074101.

4 N. Naghavi, D. Abou-Ras, N. Allsop, N. Barreau, S. Bücheler, A. Ennaoui, C.-H. Fischer, C. Guillen, D. Hariskos, J. Herrero, R. Klenk, K. Kushiya, D. Lincot, R. Menner, T. Nakada, C. Platzer-Björkman, S. Spiering, A. N. Tiwari and T. Törndahl, *Prog. Photovoltaics*, 2010, **18**, 411.

5 S. Siebentritt, *Sol. Energy*, 2004, **77**, 767.

6 A. Hultqvist, C. Platzer-Björkman, U. Zimmermann, M. Edoff and T. Törndahl, *Prog. Photovoltaics*, 2011, DOI: 10.1002/pip.1153.

7 A. Hultqvist, M. Edoff and T. Törndahl, *Prog. Photovoltaics*, 2011, **19**, 478.

8 D. C. Look, *Semicond. Sci. Technol.*, 2005, **20**, S55.

9 M. Kapilashrami, *PhD Thesis*, Royal Institute Of Technology Stockholm Sweden, 2009.

10 Y. X. Liu, Y. C. Liu, C. L. Shao and R. Mu, *J. Phys. D: Appl. Phys.*, 2004, **37**, 3025.

11 S. K. Mandal, A. K. Das, T. K. Nath and D. Karmakar, *Appl. Phys. Lett.*, 2006, **89**, 14410.

12 A. Kotani and S. Shin, *Rev. Mod. Phys.*, 2001, **73**, 203–246.

13 C. L. Dong, C. Persson, L. Vayssieres, A. Augustsson, T. Schmitt, M. Mattesini, R. Ahuja, C. L. Chang and J.-H. Guo, *Phys. Rev. B: Condens. Matter Mater. Phys.*, 2004, **70**, 195325.

14 S. Krishnamurthy, C. McGuinness, L. S. Dorneles, M. Venkatesan, J. M. D. Coey, J. G. Lunney and C. H. Pattersonb, *J. Appl. Phys.*, 2006, **99**, 08M111.

15 H. Y. Yang, S. F. Yu, S. H. Tsang, T. P. Chen, J. Gao and T. Wu, *Appl. Phys. Lett.*, 2009, **95**, 131106.

16 H. Thakur, R. Kumar, P. Thakur, N. B. Brookes, K. K. Sharma, A. Pratap Singh, Y. Kumar, S. Gautam and K. H. Chae, *Chem. Phys. Lett.*, 2011, **511**, 322.

17 J. Chouvin, J. Olivier-Fourcade, J. C. Jumas, B. Simon, Ph. Biensan, F. J. Fernández Madrigal, J. L. Tirado and C. Pérez Vicent, *J. Electroanal. Chem.*, 2000, **494**, 136.

18 S. O. Kucheyev, T. F. Baumann, P. A. Sterne, Y. M. Wang, T. van Buuren, A. V. Hamza, L. J. Terminello and T. M. Willey, *Phys. Rev. B: Condens. Matter Mater. Phys.*, 2005, **72**, 035404.

19 R. Scheer, *Trends Vac. Sci. Tech.*, 1997, **2**, 77.

20 A. Niemegeers, M. Burgelman and A. De Vos, *Appl. Phys. Lett.*, 1995, **67**, 843.

21 C. Platzer-Björkman, J. Lu, J. Kessler and L. Stolt, *Thin Solid Films*, 2003, **431–432**, 321.

22 D. Schmid, M. Ruckh and W. Schock, *Sol. Energy Mater. Sol. Cells*, 1996, **41–42**, 281.

23 E. Zawaideh, *U S. Pat*, 5 889 592, 1999.

24 A. Mendoza-Galván, C. Trejo-Cruz, J. Lee, D. Bhattacharyya, J. Metson, P. J. Evans and U. Pal, *J. Appl. Phys.*, 2006, **99**, 014306.

25 G. E. Jellison Jr. and F. A. Modine, *Appl. Phys. Lett.*, 1996, **69**, 371.

26 W. Fischer and W. L. Baun, *J. Appl. Phys.*, 1968, **39**, 4757.

This journal is © the Owner Societies 2012

Phys. Chem. Chem. Phys., 2012, **14**, 10154–10159 | 10159